engineering proceedings

MDPI

Proceeding Paper

Isothermal and Thermo-Mechanical Fatigue Life Prediction Using Total Strain Energy Density-Based Approach †

Ikram Abarkan

Department of Physics, Faculty of Sciences, Abdelmalek Essaâdi University, 93002 Tetouan, Morocco; aberkan.ikraam@gmail.com

† Presented at the 4th International Electronic Conference on Applied Sciences, 27 October–10 November 2023; Available online: https://asec2023.sciforum.net/.

Abstract: Accurate fatigue life prediction is essential for ensuring the reliability of engineering designs, particularly under thermo-mechanical fatigue conditions. This study focuses on investigating the isothermal and thermo-mechanical low-cycle fatigue of 316 FR stainless steel using finite element analysis in ABAQUS. The research evaluates the accuracy of fatigue life prediction using the total strain energy density-based approach, including Masing and non-Masing methods. The predicted results, when compared with experimental data, highlight the high accuracy of FEA in replicating cyclic behavior under both loading conditions. Additionally, the non-Masing method exhibits the highest accuracy for fatigue life prediction, particularly under isothermal loading conditions.

Keywords: thermo-mechanical fatigue; isothermal fatigue; finite element analysis; Masing and non-Masing methods; 316 FR stainless steel

Citation: Abarkan, I. Isothermal and Thermo-Mechanical Fatigue Life Prediction Using Total Strain Energy Density-Based Approach. *Eng. Proc.* **2023**, *52*, x. https://doi.org/10.3390/xxxxx

Academic Editor(s): Name

Published: date

Copyright: © 2023 by the authors. Submitted for possible open access publication under the terms and conditions of the Creative Commons Attribution (CC BY) license (https://creativecommons.org/licenses/by/4.0/).

1. Introduction

In the nuclear power industry, many components are built to operate at extreme temperatures such as those found in advanced reactor systems. Basically, repetitive heating and cooling cycles during start-up and shut down operations cause these components to be subjected to complex combined thermal and mechanical stresses. These Thermo-Mechanical Fatigue (TMF) cycles induce microscopic damage in the material, ultimately leading to crack initiation and propagation and, ultimately, structural failure, which underlines the importance of understanding TMF behavior in nuclear power systems to ensure their long-term reliability and safety.

Researchers have devoted considerable effort to developing fatigue life equations to accurately estimate the life of components subjected to low cycle fatigue (LCF) and TMF conditions. Among the most widely recognized models for estimating fatigue life are the damage summation model [1], the ductility exhaustion model [2], the frequency separation model [3], the strain range distribution model [4], and the strain energy distribution model [5]. Another commonly used fatigue life model is the total strain energy density-based model developed by Golos and Ellyin [6], which is applicable to both low- and high-cycle fatigue regimes, as well as to materials exhibiting both Masing and non-Masing behavior. A detailed explanation of these models can be found in reference [7,8]. To ensure accurate fatigue life estimation, accurate prediction of stress-strain data is required, Finite Elements Analysis (FEA) is one of the widely used technique for this purpose owing to its accuracy and effectiveness [8,9].

Generally, robust materials with excellent mechanical and thermal properties are essential to withstand repetitive loads in these components. 316 FR stainless steel stands out as an ideal choice for such applications, due to its exceptional mechanical, thermal, and low-cycle fatigue properties at elevated temperatures. In recent years, numerous research

studies have been conducted to evaluate the sustainability of 316 SS at room temperature [8–11]. However, relatively few research efforts have been dedicated to investigating the fatigue behavior of this material at higher cyclic temperature. For instance, Hormozi et al. [7] recently conducted comprehensive experimental and numerical investigations on isothermal and in-phase thermo mechanical low-cycle fatigue of 316 FR SS, both with and without hold time. Through a combination of LCF and TMF tests, they generated substantial results related to stress-strain data, cyclic plasticity behavior, and creep-fatigue damage evolution. Abarkan et al. [12] recently performed a numerical study on the cycle behavior of 316 FR SS and tested the accuracy of several fatigue life prediction models under LCF, contributing valuable insights to the understanding of this material performance.

In the literature, numerous articles have focused on evaluating the accuracy of fatigue life prediction models for 316 SS, with particular emphasis on some noteworthy contributions [8]. However, only a limited number of studies have been dedicated to investigating the accuracy of fatigue life prediction models for this material under thermo mechanical fatigue (TMF) conditions. Consequently, this research paper aims to investigate the cyclic behavior of 316 FR SS. The numerical cyclic stress-strain response is compared with the test data from [7] to assess the accuracy of FEA. Furthermore, fatigue life predictions are made for several strain amplitudes under both LCF and TMF conditions, using the total strain energy density with both Masing and non-Masing approaches. The estimated fatigue lives are then compared with the test data provided by Hormozi [7] to assess the accuracy of these predictive models.

2. Experimental Setup

Hormozi et al. [7] performed fully reversed uniaxial low-cycle tests, without a dwell period, on seven polished cylindrical specimens. These specimens had a gauge length of 8 mm and a gauge diameter of 12.5 mm, as shown in Figure 1. The TMF tests were carried out under three different applied mechanical strain amplitudes: ±0.4%, ±0.8%, and ±1.0%, within a temperature range of 500–650 °C. Whereas, the isothermal LCF experiments were performed under four different mechanical strain amplitudes, namely ±0.4%, ±0.8%, ±1.0%, and ±1.2%, at a constant temperature of 650 °C. All tests were conducted in an air environment at a consistent frequency of 0.01 Hz. Figure 2 illustrates the loading wave shape for both the TMF and isothermal LCF tests when the mechanical strain amplitude is ± 0.4%. Figure 3 illustrates the experimental configuration used for both LCF and TMF loading conditions.

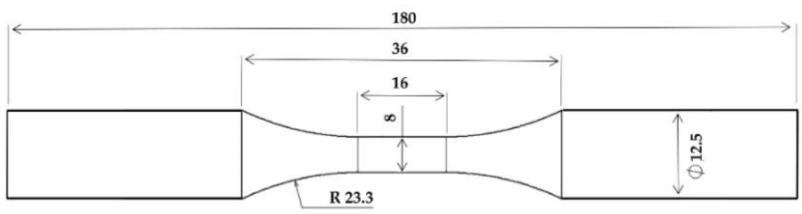

Figure 1. Geometry of the TMF and LCF specimens (all dimensions in millimeters).

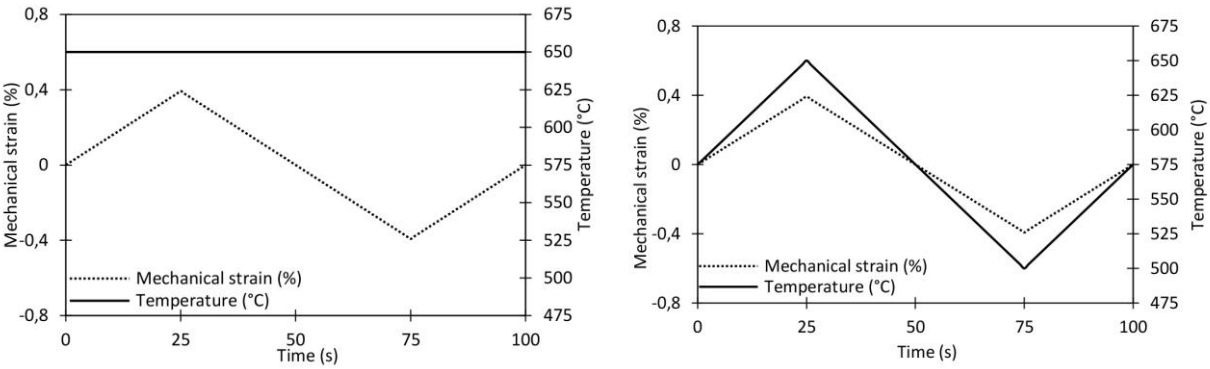

(**a**) (**b**)

Figure 2. Illustrative representation of the applied loading wave shape for (**a**) isothermal and (**b**) TMF loading.

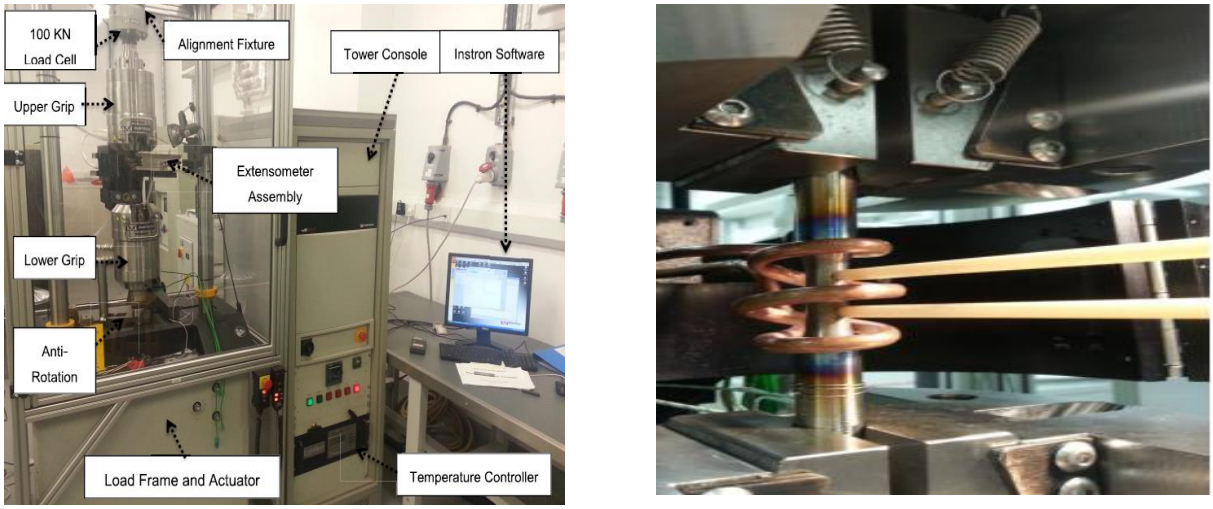

(**a**) (**b**)

Figure 3. Experimental setup for the TMF and LCF tests, with (**a**) representing the testing unit and (**b**) depicting the extensometer setup [7].

3. Finite Element Analysis

Finite element analysis (FEA) is performed on eight cylindrical specimens using ABAQUS/Standard software [12]. To reduce the computational effort and time required for FEA, A 2D-axisymmetric model with a 4 mm radius and 6.25 mm height was developed to replicate the gauge section of the samples under investigation, where the extensometer ceramic arms were positioned for the LCF and TMF experiments [7]. Symmetry boundary conditions are applied along the gauge length and gauge diameter, with prescribed cyclic displacement at the higher extremity of the 2D part, as shown in Figure 4.

CAX4R elements are selected for meshing, and a mesh sensitivity analysis was conducted to ensure that the mesh size is sufficiently small and that the results are convergent; it was found that 0.5 mm is the suitable mesh size. Besides, a fixed temperature is set at 650 °C for isothermal LCF, while it ranges from 500 to 650 °C for TMF analysis. Kinematic and isotropic plasticity data, as presented in Figure 5, along with material parameters detailed in Table 1, are implemented in the property section of ABAQUS to demonstrate the translation of the yield surface throughout the stress space (i.e., the Bauschinger effect) as well as its change in size.

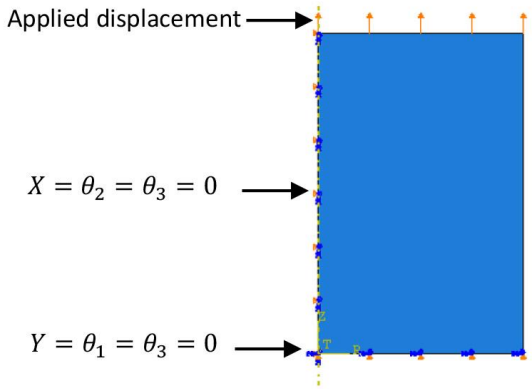

Figure 4. Representation of boundary conditions and prescribed displacement in ABAQUS.

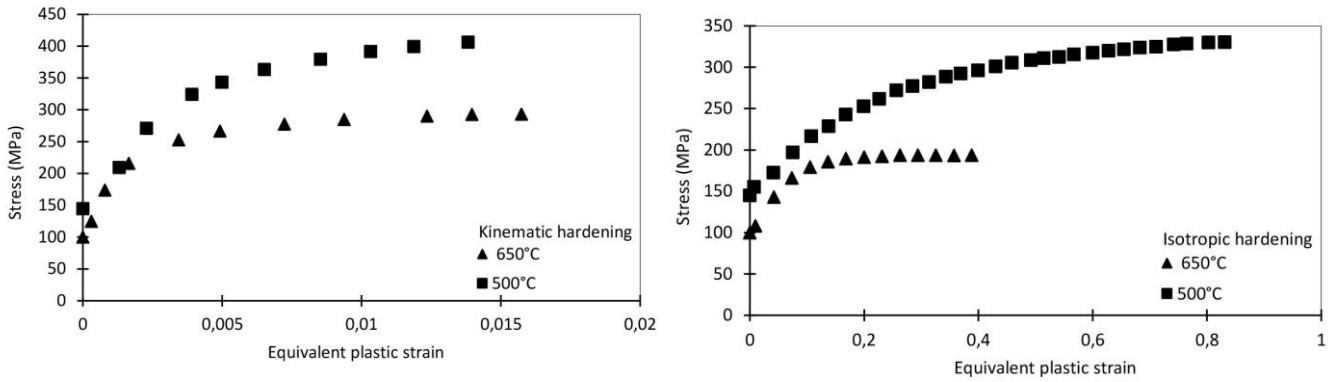

(**a**) (**b**)

Figure 5. Plasticity characterization for (**a**) Non-linear kinematic and (**a**) isotropic hardening data of 316 FR SS, at 500 and 650 °C, for a mechanical strain amplitude of ±1.0% [7].

Table 1. Material parameters of 316 FR SS at 500 and 650 °C [7].

Temperature (°C)	Young's Modulus (GPa)	Yield Strength (MPa)	Thermal Conductivity (Wm^{-1} $°C^{-1}$)	Thermal Expansion (10^{-6} $°C^{-1}$)
500	165	145	20.8	20.21
650	160	100	20	21

4. Results & Discussion

4.1. Cyclic Stress-Strain Behavior

The numerical hysteresis loops obtained at ±0.4% mechanical strain amplitude for LCF and TMF are compared to the experimental ones provided by Hormozi et al. [7]. As depicted in Figure 6, the numerically determined hysteresis loops are in excellent agreement with the experimental results for both LCF and TMF. Consequently, the generated finite element data is accurate and can be effectively employed for predicting the isothermal and thermochemical low cycle fatigue life of 316 FR SS.

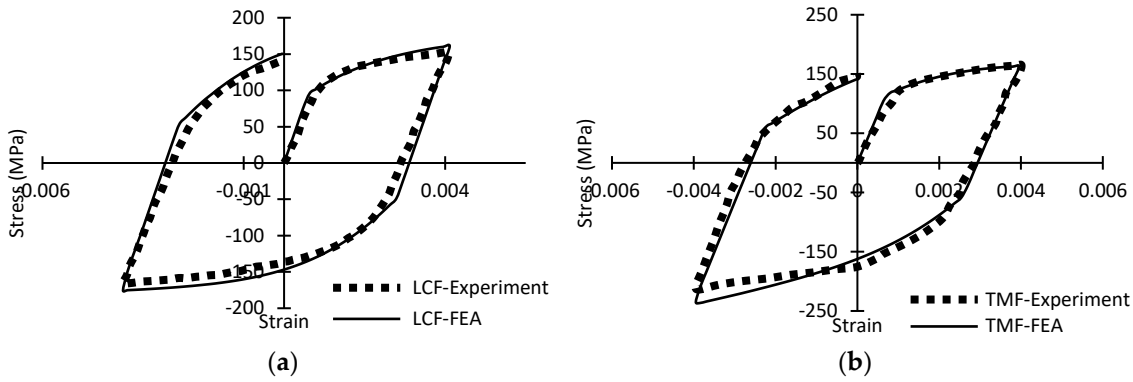

Figure 6. A comparison between the numerically obtained first hysteresis loop and the experimental one provided by Hormozi et al. [7] for: (**a**) LCF and; (**b**) TMF.

4.2. Total Strain Energy Density-Based Fatigue Life Prediction

The fatigue life can be estimated in terms of cyclic strain energy density. The total strain energy density criteria ΔW^t [13] incorporates both the plastic strain energy density ΔW^p and the elastic strain energy density ΔW^e, which is related to the tensile mode that promotes fatigue crack growth. This is expressed as follows:

$$\Delta W^t = \Delta W^p + \Delta W^e \tag{1}$$

The total strain energy density ΔW^t, as well as the plastic ΔW^p and elastic ΔW^e strain energy densities, are calculated for different applied mechanical strain amplitudes using the stabilized hysteresis loops obtained numerically. The results for the total strain energy density obtained from LCF and TMF analyses are presented in Table 2. As indicated in the table, the calculated total strain energy density falls within an error range of 6.08 and 22.29% for the LCF analysis with respect to the test data, while the total strain energy density error under TMF conditions ranges from 0.27 to 31.80%.

Table 2. The obtained total strain energy density for LCF and TMF analyses.

Strain Amplitude (%)	LCF			TMF		
	ΔW^t_{pre}	ΔW^t_{exp}	%Error	ΔW^t_{pre}	ΔW^t_{exp}	%Error
0.4	2.14	1.75	22.29	3.64	3.63	0.27
0.8	6.29	5.78	8.82	8.21	7.39	11.10
1	8.90	8.39	6.08	11.44	8.68	31.80
1.2	11.31	10.21	10.77	-	-	-

Strain energy in MPa per unit volume.

Fatigue life can be determined using the total strain energy density parameter [13] through both Masing and non-Masing analyses. The characterization of each of these two material behaviors, Masing and non-Masing, is extensively discussed in the article by Abarkan et al. [8]. In the case of Masing behavior, the expressions for the plastic and elastic strain energy density are respectively as follows [13]:

$$\Delta W^p = \left(\frac{1-n'}{1+n'}\right)\Delta\sigma\Delta\varepsilon_p \tag{2}$$

$$\Delta W^e = \frac{1}{2E}\left(\frac{\Delta\sigma}{2}+\sigma_m\right)^2 \tag{3}$$

Here, $\Delta\sigma$ represents the stress range, σ_m is the mean stress at saturation, and n' is the cyclic strain hardening exponent. By substituting Equations (2) and (3) into Equation (1), one can derive the following expression:

$$\Delta W^t = \left(\frac{1-n'}{1+n'}\right)\Delta\sigma\Delta\varepsilon_p + \frac{1}{2E}\left(\frac{\Delta\sigma}{2}+\sigma_m\right)^2 \quad (4)$$

Additionally, Coffin and Manson [14,15] and Basquin [16] introduced linear equations on the log-log scale in the low and high cycle regimes, respectively, as follows:

$$\Delta\varepsilon_p = 2\varepsilon_f'(N_f)^c \quad (5)$$

$$\Delta\sigma = 2\sigma_f'(N_f)^b \quad (6)$$

where σ_f' and b represent the fatigue strength coefficient and the fatigue strength exponent, respectively. ε_f' and c are the fatigue ductility coefficient and fatigue ductility exponent, respectively. $\Delta\sigma$ is the stress range, $\Delta\varepsilon_p$ is the plastic strain range, and N_f is the fatigue life. Moreover, the fatigue strength and ductility exponent, can be approximated to the cyclic strain hardening exponent by the following equations [17]:

$$b \cong \frac{-n'}{1+5n'} \quad (7)$$

$$c \cong \frac{-1}{1+5n'} \quad (8)$$

By substituting Equations (5)–(8) into (4), one can obtain the following expression form.

$$\Delta W^t = 4\sigma_f'\varepsilon_f'\left(\frac{c-b}{c+b}\right)(N_f)^{b+c} + \frac{1}{2E}\left[\sigma_f'(N_f)^b + \sigma_m\right]^2 \quad (9)$$

The calculation of the fatigue life N_f using the total strain energy density ΔW^t based on Masing behavior analysis can be performed using Equation (9). The values of each of the empirical parameters σ_f' ,ε_f' b and c, were determined through the least square fitting technique applied to the experimental data at 650 °C. These values are presented in Table 2. It should be noted that the LCF simulations resulted in negligible mean stress values, while TMF simulations yielded small compressive mean stresses of −12.5 MPa, −17.5 MPa, and −18 MPa for ±0.4%, ±0.8%, and ±1.0% mechanical strain amplitudes, respectively.

Table 2. Cyclic properties of 316FR SS at 650 °C.

Cyclic Strength Coefficient K'(MPa)	Cyclic Strain Hardening Exponent n'	Fatigue Strength Coefficient σ_f'(MPa)	Fatigue Strength Exponent b	Fatigue Ductility Coefficient ε_f'	Fatigue Ductility Exponent c
1171.2	0.3006	791.05	−0.178	0.5361	−0.767

As demonstrated in Figure 7a, 316 FR SS does not exhibit Masing behavior at 650 °C because the tensile portions of the experimental saturated hysteresis loops do not align on a common curve. Therefore, a Master curve was constructed by adjusting the position of the saturated hysteresis loops for each applied mechanical strain amplitude in such a way that the tensile segments of the hysteresis loops overlap and all conform to a common curve, as illustrated in Figure 7b. For non-Masing analysis, the plastic strain energy density $\Delta W^p$is expressed as follows:

$$\Delta W^p = \left(\frac{1-n}{1+n}\right)(\Delta\sigma - \delta\sigma_0)\Delta\varepsilon_p + \delta\sigma_0\Delta\varepsilon_p \quad (10)$$

The obtained values of the strain hardening coefficient K and cyclic hardening exponent n for the master curve at 650 °C, determined through least square regression, are 687.39 MPa and 0.0877, respectively. Additionally, the values of the change in proportional limit of stable hysteresis loops, δσ0, for ±0.4%, ±0.8%, and ±1.0% mechanical strain

amplitudes are 0, 92, and 122 MPa, respectively. By substituting Equations (3), (5), (6) and (10) into Equation (1), the following expression was derived [13]:

$$\Delta W^t = 4\sigma_f'\varepsilon_f'\left(\frac{1-n}{1+n}\right)(N_f)^{b+c} + \left(\frac{4n}{1+n}\right)\delta\sigma_0\varepsilon_f'(N_f)^c + \frac{1}{2E}\left[\sigma_f'(N_f)^b + \sigma_m\right]^2 \quad (11)$$

Therefore, Equation (11) is utilized to predict the number of cycles to failure using non-Masing analysis, both under isothermal and in-phase thermo mechanical fatigue loading conditions.

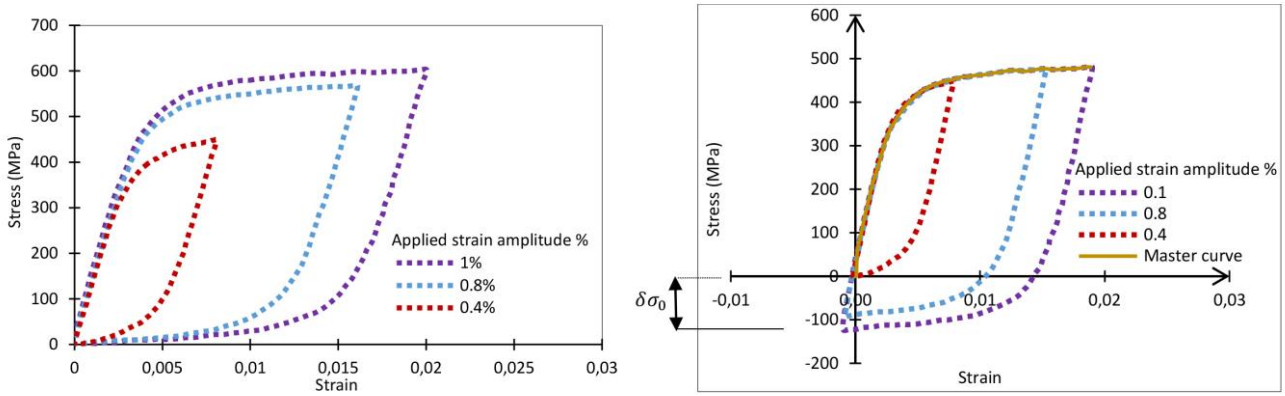

(**a**) (**b**)

Figure 7. (**a**) Experimental saturated hysteresis loops provided by Hormozi et al. [7] after aligning compressive tips at the origin, (**b**) Generation of the master curve for non-Masing behavior in 316 FR SS at 650 °C.

The estimated isothermal and thermo-mechanical fatigue life under ±0.4%, ±0.8%, ±1.0%, and ±1.2% applied mechanical strain amplitudes, using Masing and non-Masing methods (i.e., Equations (9) and (11), respectively), are compared against the experimental results. As depicted in Figure 8a,b, the obtained predictions for low-cycle fatigue and thermo-mechanical fatigue life from both equations are conservative. In other words, the predicted LCF and TMF life using Masing analysis are within a factor of 1.5 and 3.5, respectively, while in the case of non-Masing analysis, they are close to a factor of 1 and 2.5, respectively. Even with the use of these two analyses, conservative life predictions were observed for both LCF and TMF conditions. The present results demonstrate that both Masing and non-Masing analyses provide better estimates of cyclic life under LCF compared to TMF conditions, with the non-Masing model yields more realistic estimation. The same pattern was identified in the study conducted by Abarkan et al. [8] regarding the low-cycle fatigue (LCF) of 316LN stainless steel at room temperature. Their findings indicated that fatigue life predictions derived from non-Masing models exhibited better agreement with experimental results than those produced by the Masing model, for both high and low strain amplitudes, and that the Masing model yields conservative fatigue life estimates, whereas the non-Masing model offers a more accurate prediction of fatigue life.

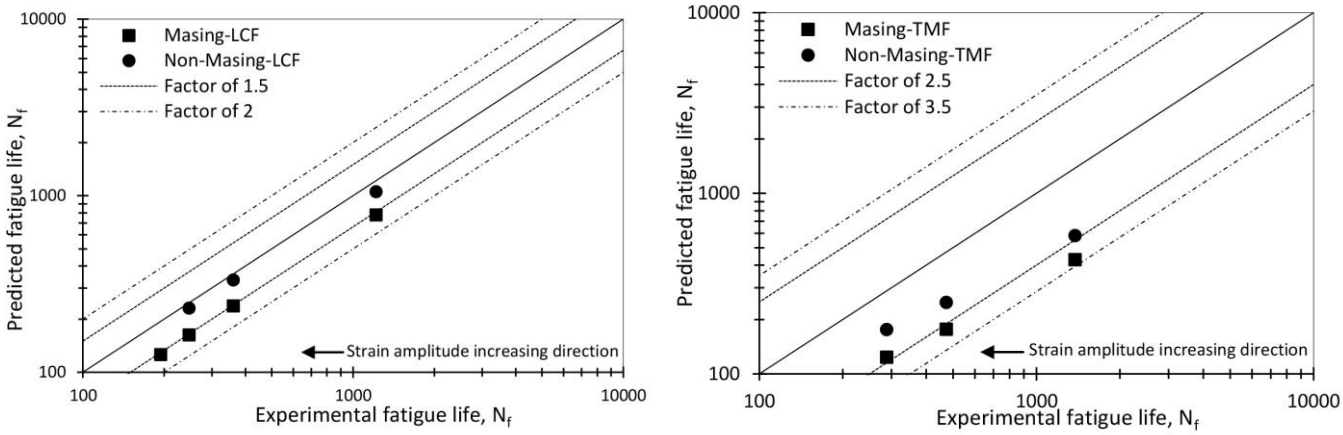

(**a**) (**b**)

Figure 8. Comparison between the predicted fatigue life through Masing and non-Masing analyses and the experimental data, (a) under LCF and (b) under TMF.

5. Conclusion Remarks

In this study, the low cycle fatigue life has been predicted under isothermal and in-phase thermo mechanical fatigue at various strain amplitude levels using the total strain energy density approach with both Masing and non-Masing methods. These predictions have been compared to experimental data to assess their accuracy, and the following conclusions and remarks have been made; (1): The cyclic stress-strain response was accurately replicated by finite element analysis (FEA), providing satisfactory results for the total strain energy density for both loading conditions; (2): The fatigue life equation parameters, determined through least square regression analysis, have been provided; (3): The non-Masing method was found to achieve the most accurate fatigue life predictions when compared to the Masing method, demonstrating higher accuracy for isothermal loading compared to TMF.

Funding: This research received no external funding.

Institutional Review Board Statement: Not applicable.

Informed Consent Statement: Not applicable.

Data Availability Statement: Data can be made available on demand.

Conflicts of Interest: The author declares no conflict of interest.

References

1. Taira, S. Lifetime of structures subjected to varying load and temperature. In *Creep in Structures*; Springer: Berlin/Heidelberg, Germany, 1962; pp. 96–124.
2. Priest, R.H.; Ellison, E.G. A combined deformation map-ductility exhaustion approach to creep-fatigue analysis. *Mater. Sci. Eng.* **1981**, *49*, 7–17. https://doi.org/10.1016/0025-5416(81)90128-2.
3. Coffin, L.F. *Concept of Frequency Separation in Life Prediction for Time-Dependent Fatigue*; No. CONF-761107-14; General Electric Co.: Schenectady, NY, USA, 1976.
4. Manson, S.S.; Halford, G.R.; Hirschberg. M.H. *Creep Fatigue Analysis by Strain-Range Partitioning*; NASA: Washington, DC, USA, 1971.
5. He, J.; Duan, Z.; Ning, Y.; Zhao, D. Strain Energy Partitioning and Its Application to GH33A Ni-Base Superalloy and 1Cr18Ni9Ti Stainless steel. *Acta Metall. Sin.* **1985**, *21*, 54–63.
6. Golos, K.; Ellyin, F. Total strain energy density as a fatigue damage parameter. In *Advances in Fatigue Science and Technology*; Springer: Dordrecht, The Netherlands, 1989; Volume 159, pp. 849–858.
7. Hormozi, R. Experimental and Numerical Simulations of Type 316 Stainless Steel Failure under LCF/TMF Loading Conditions. Ph.D. Thesis, Imperial College, London, UK, 2014.
8. Abarkan, I.; Shamass, R.; Achegaf, Z.; Khamlichi, A. Numerical and analytical studies of low cycle fatigue behavior of 316 LN austenitic stainless steel. *J. Press. Vessel. Technol.* **2020**, *144*, 061507.

9. Abarkan, I.; Khamlichi, A.; Shamass, R. A Study on low cycle fatigue life assessment of notched specimens made of 316 LN austenitic stainless steel. *J. Press. Vessel. Technol.* **2022**, *144*, 021503.
10. Roy, S.C.; Goyal, S.; Sandhya, R.; Ray, S. Low cycle fatigue life prediction of 316 L(N) stainless steel based on cyclic elasto-plastic response. *Nucl. Eng. Des.* **2012**, *253*, 219–225.
11. Dutta, A.; Dhar, S.; Acharyya, S.K. Material characterization of SS 316 in low-cycle fatigue loading. *J. Mater. Sci.* **2010**, *45*, 1782–1789.
12. *ABAQUS/Standard*, version 6.14; Dassault Systèmes Simulia Corp.: Providence, RI, USA, 2014.
13. Golos, K.; Ellyin, F. Total strain energy density as a fatigue damage parameter. In *Advances in Fatigue Science and Technology*; Springer: Dordrecht, The Netherlands, 1989; pp. 849–858.
14. Coffin, L.F., Jr. *A Study of the Effects of Cyclic Thermal Stresses on a Ductile Metal*; Knolls Atomic Power Laboratory: Schenectady, NY, USA, 1953.
15. Manson, S.S. *Behavior of Materials Under Conditions of Thermal Stress*; NASA: Washington, DC, USA, 1954.
16. Basquin, O.H. The exponential law of endurance tests. *Proc. Am. Soc. Test. Mater.* **1910**, *10*, 625–630.
17. Morrow, J. Cyclic plastic strain energy and fatigue of metals. In *Internal Friction, Damping, and Cyclic Plasticity*; ASTM International: West Conshohocken, PA, USA, 1965.

Disclaimer/Publisher's Note: The statements, opinions and data contained in all publications are solely those of the individual author(s) and contributor(s) and not of MDPI and/or the editor(s). MDPI and/or the editor(s) disclaim responsibility for any injury to people or property resulting from any ideas, methods, instructions or products referred to in the content.